materials

MDPI

Article

Brillouin Scattering Study of Ferroelectric Instability of Calcium–Strontium–Barium Niobate Single Crystals

Seiji Kojima [1,*], Md Aftabuzzaman [1,2], Jan Dec [3] and Wolfgang Kleemann [4]

[1] Division of Materials Science, University of Tsukuba, Tsukuba 305-8573, Japan
[2] Department of Physics, Pabna University of Science and Technology, Pabna 6600, Bangladesh
[3] Institute of Materials Science, University of Silesia, PL-40-007 Katowice, Poland
[4] Angewandte Physik, University of Duisburg-Essen, D-47048 Duisburg, Germany
* Correspondence: kojima@ims.tsukuba.ac.jp

Abstract: Uniaxial ferroelectrics with tetragonal tungsten bronze structure are important functional materials with photorefractive, electrooptic, piezoelectric, and pyroelectric properties. $Sr_xBa_{1-x}Nb_2O_6$ (SBN100x) with $x > 50$ is known as a typical uniaxial relaxor ferroelectric, while $Ca_xBa_{1-x}Nb_2O_6$ (CBN100x) undergoes nearly normal ferroelectric phase transitions. Single crystals of CSBN100x = [x(CBN28) + (1 − x) (SBN61)] = $x Ca_{0.28}Ba_{0.72}Nb_2O_6$ + (1 − x) $Sr_{0.61}Ba_{0.39}Nb_2O_6$ with nominal x = 0.00, 0.25, 0.50, 0.75, and 1.00 were studied to clarify the dynamical properties at the crossover from relaxor (x = 0) to normal (x = 1) ferroelectric behavior. The longitudinal acoustic (LA) and transverse acoustic (TA) modes and a central peak (CP) related to the relaxation process of polarization fluctuations along the polar c-axis were studied in uniaxial ferroelectric CSBN single crystals as a function of temperature via Brillouin scattering spectroscopy. A CBN28 (x = 1.00) crystal shows the sharp elastic anomaly of the LA mode in the gigahertz range toward Curie temperature, T_c. However, those of CSBN25 (x = 0.25) and SBN61 (x = 0.00) crystals show diffusive anomalies due to stronger random fields. The relaxation time determined from the width of a CP shows a critical slowing down in the vicinity of T_c. The elastic anomaly and slowing down of relaxation time of CSBN100x crystals become diffusive in the vicinity of T_c as the CBN28 content decreases. The origin of the crossover from relaxor to normal ferroelectric phase transitions is discussed in terms of the difference in the A1 and A2 sites' occupancies.

Keywords: Brillouin scattering; ferroelectric; relaxor; acoustic modes; elastic properties; slowing down

check for updates

Citation: Kojima, S.; Aftabuzzaman, M.; Dec, J.; Kleemann, W. Brillouin Scattering Study of Ferroelectric Instability of Calcium–Strontium–Barium Niobate Single Crystals. *Materials* **2023**, *16*, 2502. https://doi.org/10.3390/ma16062502

Academic Editor: Georgios C. Psarras

Received: 16 February 2023
Revised: 16 March 2023
Accepted: 19 March 2023
Published: 21 March 2023

Copyright: © 2023 by the authors. Licensee MDPI, Basel, Switzerland. This article is an open access article distributed under the terms and conditions of the Creative Commons Attribution (CC BY) license (https://creativecommons.org/licenses/by/4.0/).

1. Introduction

Ferroelectricity is defined by the existence of a spontaneous polarization, the direction of which is switchable by an external electric field [1]. Uniaxial ferroelectric materials with a tetragonal tungsten bronze (TTB) structure are technologically important for optical applications involving electro-optic, nonlinear optic, photorefractive, pyroelectric, and piezoelectric properties [2]. In light of recent environmental problems, Pb-free ferroelectrics and their functional properties have become important [3]. In TTB ferroelectrics, the direction of spontaneous polarization is restricted to the polar c-axis, which is why they are also called uniaxial ferroelectrics [4]. The structural formula of TTB ferroelectrics is expressed by $(A1)_2(A2)_4(C)_4$-$(B1)_2(B2)_8O_{30}$, with corner-sharing distorted BO_6 octahedra as shown in Figure 1. The smallest C site is occupied only by Li, such as in $K_3Li_2Nb_5O_{15}$(KLN). In ferroelectric $Ba_2NaNb_5O_{15}$ (BNN), which is well known by its excellent second harmonic generation, all the A1 and A2 sites are occupied by Ba^{2+} and Na^{1+} ions, respectively. BNN belongs to the filled TTB ferroelectrics due to their complete occupation of A1 and A2 sites and undergoes a normal ferroelectric phase transition with a sharp dielectric anomaly in the vicinity of a ferroelectric Curie temperature, T_c, which is the highest among TTB ferroelectrics [2,5]. In contrast, the A1 sites of $Sr_xBa_{1-x}Nb_2O_6$ (SBN100x) are occupied in

part by Sr^{2+} ions, and the A2 sites are occupied in part by both Ba^{2+} and Sr^{2+} ions. Since 1/6 (A1 + A2) sites remain unoccupied, it belongs to the so-called unfilled (open) TTB ferroelectrics due to the incomplete occupancy of A1 and A2 sites. The empty A1 and/or A2 sites cause the charge disorder and are the main sources of quenched random fields (RFs), which enhance the relaxor features characterized by the frequency dispersion of dielectric susceptibility and diffusive phase transition [6,7]. In SBN, the strength of RFs increases as the Sr content of smaller (1.12 Å) Sr^{2+} ions increases, and SBN has attracted much attention as a typical uniaxial relaxor ferroelectric [8].

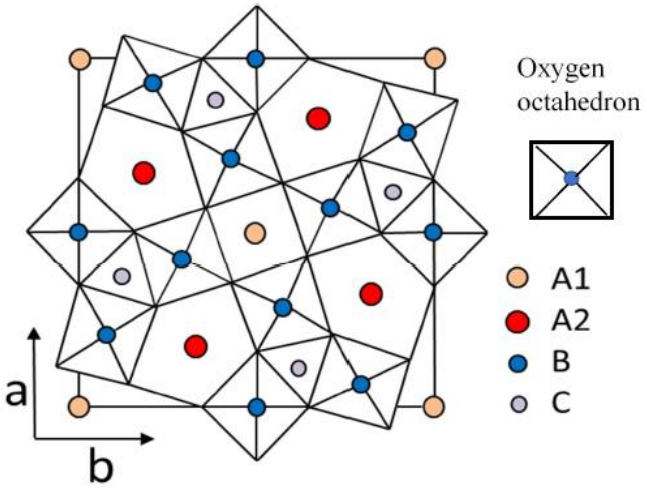

Figure 1. Crystal structure of *ab* plane, which is perpendicular to the polar *c*-axis, in tetragonal tungsten bronze ferroelectrics. There are three different interstices (two square A1, four pentagonal A2, and four trigonal C sites in a unit cell).

The disadvantage of SBN in application is the relatively low Curie temperatures. The $Ca_xBa_{1-x}Nb_2O_6$ (CBN100x) compounds also belong to the unfilled TTB structure and show quite similar physical properties to SBN, while their Curie temperatures are much higher than those of SBN [9]. Therefore, the excellent optical and ferroelectric properties of CBN make them potential candidates for applications at relatively high temperatures [10]. Recently, CBN nanopowders were synthesized. Their analysis of the various optical properties, especially the photorefractive effect, suggests that CBN nanopowders can be potentially applied for ultrahigh-density optical data storage [11]. In CBN, most of the smaller (0.99 Å) Ca^{2+} ions occupy A1 sites, whereas the relatively larger (1.34 Å) Ba^{2+} ions predominantly occupy the A2 sites [12,13]. Thus, in contrast to SBN with strong RFs, the lower degree of disorder of the Ca^{2+} and Ba^{2+} ions of CBN causes the weak RFs, and the diffusive nature of CBN is weaker than that of SBN [14]. In the Brillouin scattering study of CBN28, the intense central peak (CP) caused by polarization fluctuations along the *c*-axis was clearly observed in the vicinity of T_c. The relaxation time determined by the CP width clearly shows critical slowing down towards T_c, reflecting a weakly first-order phase transition under weak RFs [15].

Within the quasi-ternary $CaNb_2O_6$-$SrNb_2O_6$-$BaNb_2O_6$ system, selected $Ca_xSr_yBa_{1-x-y}Nb_2O_6$ (CSBN) compounds were grown via the Czochralski method in a tungsten–bronze-type structure [16]. The solid solution of CSBN is technologically important due to the coexistence of the high T_c of CBN and excellent functionality of SBN. In fundamental science, the crossover of CSBN from weak RFs of CBN with a nearly normal ferroelectric nature to strong RFs of SBN with a relaxor nature is very interesting regarding control of the strength of RFs only by Ca content. Since there are three kinds of cations, Ca^{2+}, Sr^{2+}, and Ba^{2+}, with increasing ionic radii occupying A1 and A2 sites, the degree of freedom to control physical properties increases. The Curie temperatures of xCBN28-(1 − x) SBN61 (CSBN100x) are shown in Figure 2. As the Ca content increases in CSBN, T_c monotonically increases, and the ferroelectric phase transition becomes less

diffusive due to the decrease of disorder, which indicates the suppression of the RFs [17,18]. In addition, it is worth mentioning here that the above composition formula of the CSBN system may be expressed in a more compact fashion: (i) $x = 0$, $Sr_{0.61}Ba_{0.39}Nb_2O_6$ for SBN61, (ii) $x = 0.25$, $Ca_{0.07}Sr_{0.458}Ba_{0.472}Nb_2O_6$ for CSBN25, (iii) $x = 0.50$, $Ca_{0.14}Sr_{0.305}Ba_{0.555}Nb_2O_6$ for CSBN50, (iv) $x = 0.75$, $Ca_{0.21}Sr_{0.153}Ba_{0.637}Nb_2O_6$ for CSBN75, and (v) $x = 1.00$, $Ca_{0.28}Ba_{0.72}Nb_2O_6$ for CBN28.

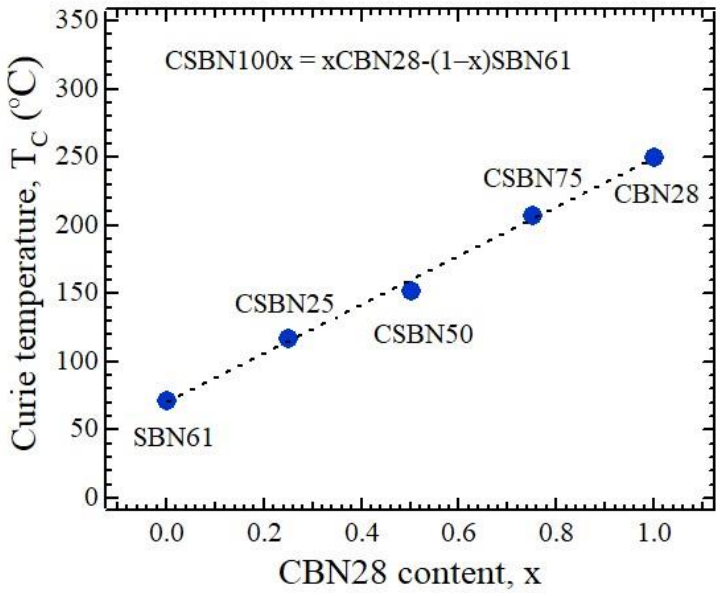

Figure 2. Ferroelectric Curie temperatures of calcium strontium barium niobate crystals with TTB structure. The dotted line is a linear fitting.

Brillouin scattering is the inelastic light scattering by thermally excited sound waves and has been used as a non-contact and non-destructive method to obtain elastic constants in the gigahertz range [19]. In the present study, the elastic properties and dynamical instability of CSBN100*x* crystals were investigated by using Brillouin scattering spectroscopy.

2. Experimental Methods

CSBN100*x* single crystals were grown via the Czochralski method [16] for the nominal compositions, $x = 0.00, 0.25, 0.5, 0.75, 1.00$. The CSBN single crystals were grown at the Institute of Electronic Materials Technology (Poland) under the guidance of Prof. T. Lukasiewicz. Their structural measurements were published [20,21]. The real composition of the crystals obtained was checked with the use of ICP-OES (inductively coupled plasma–optical emission spectroscopy) method and the result was published [22]. It has appeared that the real composition was, within uncertainties, satisfactorily close to the established one. Single crystalline plates were cut along [100] (*a*-plate) and [001] (*c*-plate) with optically polished 5×5 mm^2 surfaces and 1 mm thickness. Brillouin scattering spectra were measured at the back scattering geometry using a high-contrast 3 + 3 passes tandem Fabry–Perot interferometer, as shown in Figure 3 [19]. The exciting source was a diode-pumped solid state (DPSS) laser with a wavelength of 532 nm and a power of 100 mW. Scattered light was detected using a photon counting system. The specimen's temperature was controlled using a cooling/heating stage (Linkham, THMS600, Salfords, UK) with a stability of ±0.1 °C. Using an *a*-plate, longitudinal acoustic (LA) and transverse acoustic (TA) modes–which propagate along the *a*-axis—and the CP of polarization fluctuations along the ferroelectric *c*-axis were measured. Using a *c*-plate, LA and TA modes—which propagate along the *c*-axis—were measured.

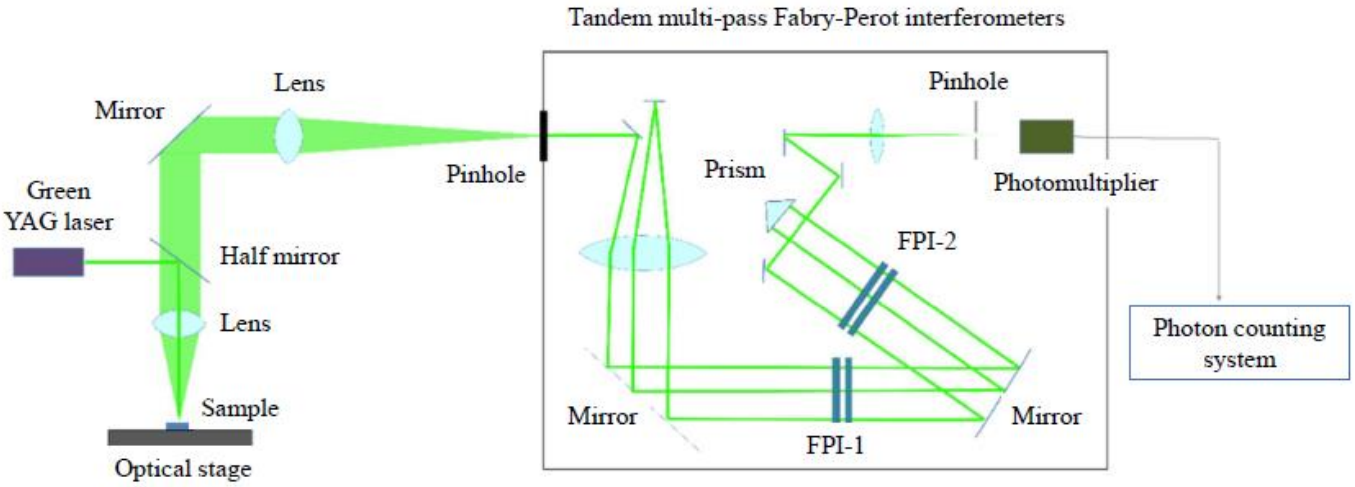

Figure 3. Schematic illustration of experimental setup of Brillouin scattering measurement with tandem multipass Fabry–Perot interferometers.

3. Results and Discussion

3.1. Elastic Anomaly of LA Modes

The temperature dependences of Brillouin scattering spectra of a CSBN50 crystal measured at the backward scattering geometry using *a*- and *c*-plates are shown in Figures 4 and 5, respectively. The direction of the wave vector of a scattered phonon is parallel to the *a*-axis for an *a*-plate and to the *c*-axis for a *c*-plate. The spectrum at 160 °C in Figure 4 shows doublets of TA and LA modes which propagate along the *a*-axis at about 32 and 59 GHz, respectively. The broad Rayleigh wings observed at 0 GHz are a CP with $A_1(z)$ symmetry, which is related to the polarization fluctuations along the ferroelectric *c*-axis. The maximum of intensity of a CP was observed at 152 °C. The spectrum at 160 °C in Figure 5 shows TA and LA modes which propagate along the *c*-axis at about 32 and 48 GHz, respectively. However, a CP related to the polarization fluctuations in the *ab*-plane, which is perpendicular to the ferroelectric *c*-axis, was not observed at all the temperatures.

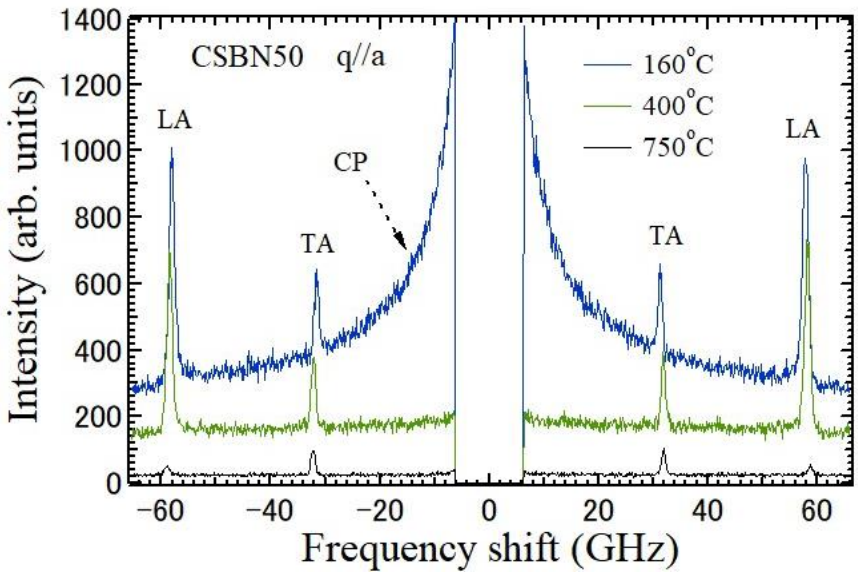

Figure 4. Temperature dependences of Brillouin scattering spectra measured by backward scattering geometry using the *a*-plate of a CSBN50 crystal. The wave vector *q* of the scattered phonon is parallel to the *a*-axis. Doublets of TA and LA modes which propagate along the *a*-axis were also observed. An intense CP was observed at zero frequency shift.

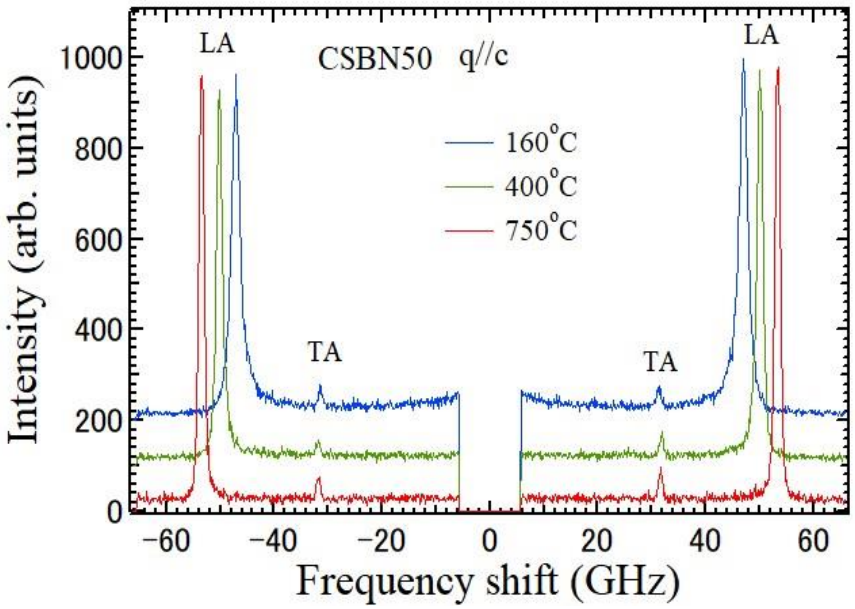

Figure 5. Temperature dependence of Brillouin scattering spectra measured by backward scattering geometry using the *c*-plate of a CSBN50 crystal. The wave vector q of the scattered phonon is parallel to the *c*-axis. Doublets of TA and LA modes which propagate along the *c*-axis were observed. No CP was observed.

The measured Brillouin spectra were fitted using Voigt functions, a convolution of Lorentzian and Gaussian functions, for which the width of the Gaussian function was fixed as an instrumental function. The temperature dependence of frequency shift and width of the LA mode, which propagates along the ferroelectric *c*-axis, were determined by the fitting, as shown in Figure 6. Upon cooling from the high temperature above the Burns temperature, T_B = 520 °C, the LA frequency shows the remarkable softening toward T_c = 152 °C. Upon cooling from the high temperature, the LA mode width shows a remarkable increase toward T_c. Such an elastic anomaly is related to the temperature evolution of polar nanoregions (PNRs) triggered by the RFs [15,23]. In the ferroelectric phase, the width gradually decreases due to the freezing of PNRs into stable nanodomains.

In lead-based relaxor ferroelectrics with perovskite structure, it is known that T_B = 427 °C and the intermediate temperature, T^* = 227 °C, are unaffected by compositions [24]. In SBN, T_B = 350 °C and T^* = 190 °C are unaffected by compositions of Sr ions, and in CBN, T_B = 517 °C and T^* = 367 °C are unaffected by compositions of Ca ions [23]. In CSBN—if we assume linear change in T_B and T^* for the composition dependence—T_B = 434 °C and T^* = 279 °C are expected for CSBN50, as shown in Figure 6. Upon cooling, the dynamic–static transition and rapid growth PNRs occur at T^*, and the remarkable decrease of the LA frequency and an increase in LA width occur towards T_C due to the scattering of LA phonons by PNRs.

The sound velocity, V, is determined by the frequency shift ν_B in the Brillouin scattering spectrum using the equation:

$$V = \frac{\lambda_i \upsilon_B}{2n \sin\frac{\theta}{2}} \quad (1)$$

where λ_i, θ, and n are the wavelength of an incident beam, the scattering angle, and the refractive index of the sample, respectively. The velocity is determined from the frequency shift. The attenuation, α, is determined using

$$\alpha = \frac{\pi\Gamma}{V} \quad (2)$$

where Γ is the FWHM of the Brillouin peak [25]. The dispersions of refractive indices and the Curie temperatures were determined in CSBN100x crystals grown using the Czochralski method [26]. The temperature dependences of LA velocity and LA attenuation calculated

from the LA shift and width for five CSBN crystals using the values of refractive indices [26] are shown in Figures 7 and 8, respectively. The LA velocity and attenuation of CBN28 with very weak RFs show remarkable changes in the vicinity of T_C = 254 °C and a sharp minimum in the LA velocity. In contrast, in SBN61, with strong RFs, the temperature dependence of the LA velocity and the attenuation in the vicinity of T_C = 72 °C are diffusive in the vicinity of T_C. These differences can be caused by the variation in the strength of RFs, which suppress the sharp changes in the vicinity of T_C. The temperature dependences of LA velocity and attenuation gradually change as the CBN28 content decreases from normal ferroelectric, such as CBN28, to relaxor SBN61. This crossover was also reported on the dielectric properties of CSBN ceramics [27]. Such a crossover from normal to relaxor ferroelectrics was also studied in SBN from Ba- to Sr- rich regions [7,28,29]. Recently, the crossover from normal to relaxor nature in SBN and CSBN ceramics was studied by the Rietveld refinement of X-ray diffraction and Raman spectroscopy [18]. The observed site occupancies at A1 and A2 sites were analyzed using residual entropy calculations. It was concluded that the origin of the crossover is directly related to the majority of A2 sites being occupied by Ba^{2+}.

Among elastic constants, the coupling between c_{33} and the polarization fluctuations along the ferroelectric c-axis is very strong, while the coupling between other elastic constants and the order parameters of a ferroelectric phase transition is very week. Consequently, the elastic anomaly of other elastic constants is very small, and it is difficult to discuss the dynamical properties of a phase transition using the other two elastic constants. Therefore, the elastic anomaly of c_{33} was analyzed. The difference in temperature dependences of the elastic stiffness constant $c_{33} = \rho V_{LA}^2$ between CBN28 and CSBN75 is shown in Figure 9a,b, respectively, where ρ and V_{LA} are the density and LA velocity of Figure 7, respectively. In comparison with the remarkable softening of elastic constant of CBN28 towards T_c, that of CSBN25 is suppressed, and the anomaly becomes diffusive. The elastic anomaly of perovskite ferroelectrics was analyzed by the following equation in the paraelectric phase.

$$c_{ij}(t) = c_{ij}^0 + c_{ij}^1 T - c_{ij}^2 \left(\frac{T - T_0}{T_0} \right)^{-n}, \text{for } T_0 \leq T_c \leq T. \quad (3)$$

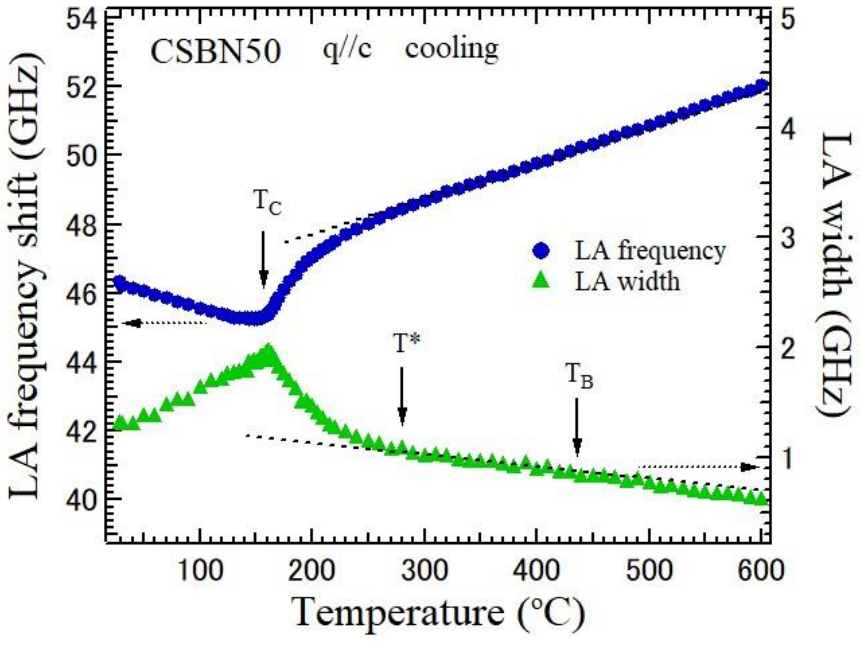

Figure 6. Temperature dependence of LA frequency shift and width along the ferroelectric *c*-axis of a CSBN50 crystal on cooling. The dotted lines show the nearly linear temperature dependences at high temperatures. T*and T_B are the intermediate and Burns temperatures, respectively. The dotted line arrows indicate the corresponding *y*-axis.

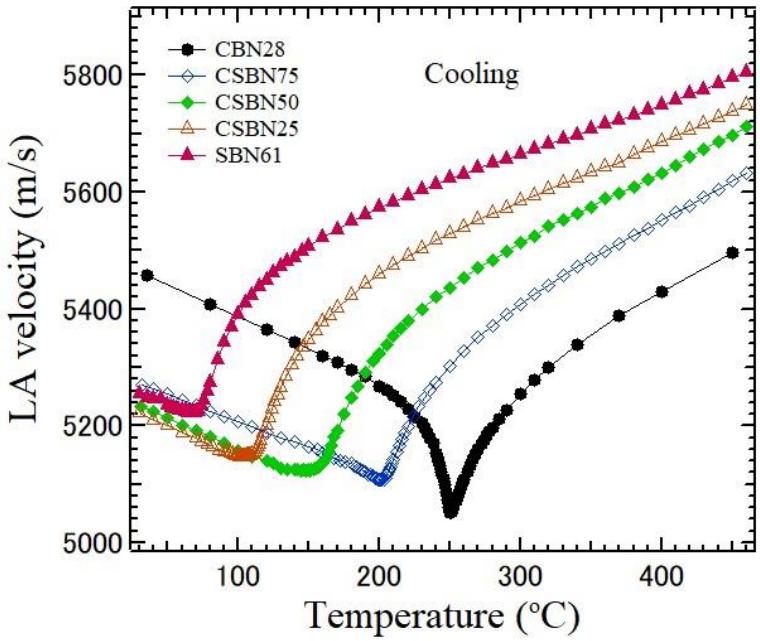

Figure 7. Temperature dependences of LA velocity which propagates along the ferroelectric *c*-axis of five CSBN100*x* crystals on cooling. As the CBN28 content decreases, the change in LA velocity becomes diffusive in the vicinity of T_c.

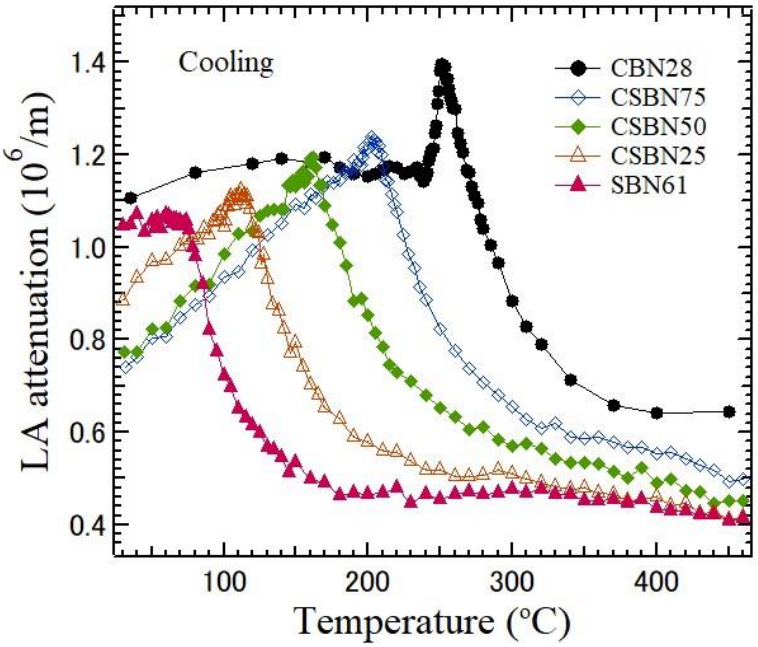

Figure 8. Temperature dependences of LA attenuation, which propagates along the ferroelectric *c*-axis of five CSBN100*x* crystals on cooling. As the CBN28 content decreases, the change in LA attenuation becomes diffusive in the vicinity of T_c.

Here, c_{ij}^0, c_{ij}^1, and c_{ij}^2 are constants. On the right-hand side, the second term is the anharmonic effect and the third term is the elastic anomaly caused by the fluctuations in the order parameter. The critical exponent, n, was predicted to be 0.5 for three-dimensional fluctuations, 1.0 for two-dimensional fluctuations, and 1.5 for one-dimensional fluctuation of the order parameters [30]. For example, for undoped and Li-doped $K(Ta_{0.6}Nb_{0.4})TiO_3$ crystals with perovskite structure, the observed exponent of n = 0.5 indicates the three-dimensional fluctuations of polarization, which are related to the 8-site model of the

off-center of B-site ions along the eight equivalent [111] directions [31]. In CBN28, the fitted value of n = 1.52 indicates the one-dimensional fluctuations in polarization along the [001] axis, which is suitable for a uniaxial ferroelectric phase transition. In CSBN75, the fitted value n = 2.17 shows the deviation from the value of theoretical model, in which structural disorder was not considered. The origin of the deviation from n = 1.5 in CSBN75 is probably attributed to the diffusive nature induced by the RFs.

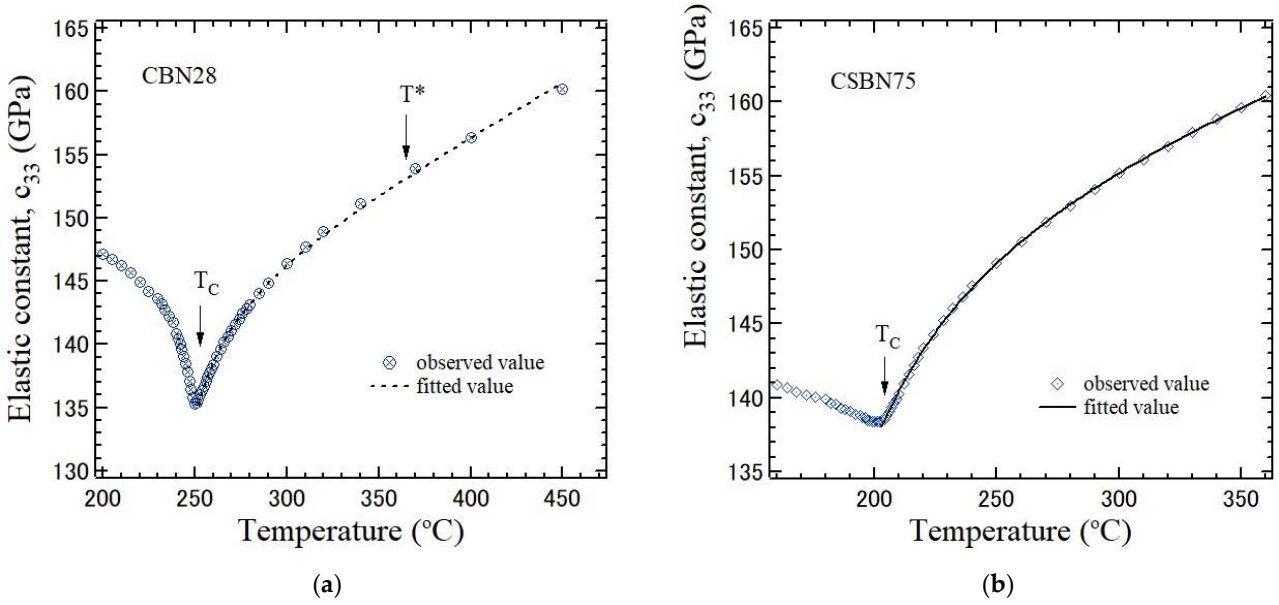

Figure 9. Difference in the temperature dependences of the elastic stiffness constant c_{33} between (**a**) CBN28 and (**b**) CSBN75 crystals. The elastic constant of CBN28 shows a sharp anomaly in the vicinity of T_C, while that of CSBN75 shows the diffusive nature and that the elastic anomaly is smaller. The solid lines in a paraelectric phase are curves fitted using Equation (3).

3.2. Critical Slowing down Observed by a Central Peak

The relaxation process of the polarization fluctuations along a ferroelectric *c*-axis has been observed from the width of the narrow CP in CBN28 [15]. Temperature dependences of relaxation time determined from the width of a narrow central peak observed using *a*-plates of five CSBN crystals were analyzed. In CBN28, the temperature dependences of relaxation time of polarization fluctuations determined by a central peak along the *c*-axis show the critical slowing down toward T_C. However, as the CBN28 content decreases, the slowing down is stretched by the strengthened RFs. In relaxor ferroelectrics, the dielectric constant ε obeys the extended Curie–Weiss law based on the compositional heterogeneity model as below [32].

$$\frac{1}{\varepsilon} = \frac{1}{\varepsilon_0} + \frac{1}{\varepsilon_1}\left(\frac{T - T_C}{T_C}\right)^{\gamma}, \quad \text{for } T > T_c. \tag{4}$$

Here, ε_0 and ε_1 are constants and γ is the diffuseness exponent. The case of γ = 1 refers to the Curie–Weiss law for a normal ferroelectric phase transition, and that of γ = 2 is a typical relaxor phase transition. For a partially disordered ferroelectric phase transition, it holds $1 < \gamma \leq 2$. In Nb-doped $Pb(Zr_{0.75}Ti_{0.25})O_3$ ceramics, γ = 1.5 was reported [33]. The dielectric properties of CSBN crystals showed that a relaxor nature with noticeable dielectric dispersion was observed in CSBN25 [22]. The origin of its relaxor properties was attributed to lower excess oxygen in CSBN25.

In an order–disorder ferroelectric phase transition, the relaxation time τ shows critical slowing down towards T_c. However, in the ferroelectric phase transitions of relaxor ferroelectrics, the diffusive nature was observed in the critical slowing down [34]. In $0.93Pb(Zn_{1/3}Nb_{2/3})O_3$-$0.07PbTiO_3$ (PZN-7PT), the slowing down was suppressed below the intermediate temperature T^* and typical critical slowing down was not observed

near T_c [35]. The local transition from dynamic to static PNRs at T^* suppresses further slowing down. To describe such a suppressed slowing down by RFs, an empirical equation of the stretched slowing down was used in the vicinity of T_c, as given by the following equation [35],

$$\frac{1}{\tau_{CP}} = \frac{1}{\tau_0} + \frac{1}{\tau_1}\left(\frac{T - T_C}{T_C}\right)^{\beta}, \quad \text{for } T > T_c. \tag{5}$$

where β is the stretched exponent. In the case of β = 1.0, Equation (5) gives the critical slowing down of normal ferroelectrics. Regarding TTB ferroelectrics, β = 1.0 was reported for BNN [36] and CBN28 [15]. In the case of β > 1.0, the slowing down of relaxation time is suppressed and/or stretched by the increase of the strength of RFs. In PMN-17PT and PMN-56PT, the observed values are β = 2.12 and 1.43, respectively [37]. RFs of PMN-17PT are stronger than those of PMN-56PT.

The difference in the temperature dependences of the stretched slowing down is shown in Figure 10 between CSBN75 and CSBN50 crystals. The dotted lines are values fitted using Equation (5) with β = 1.53 for CSBN75 and β = 1.88 for CSBN50 in a paraelectric phase. Therefore, as the CBN28 content decreases, the stretched exponent increases monotonically from β = 1 of the normal ferroelectric case.

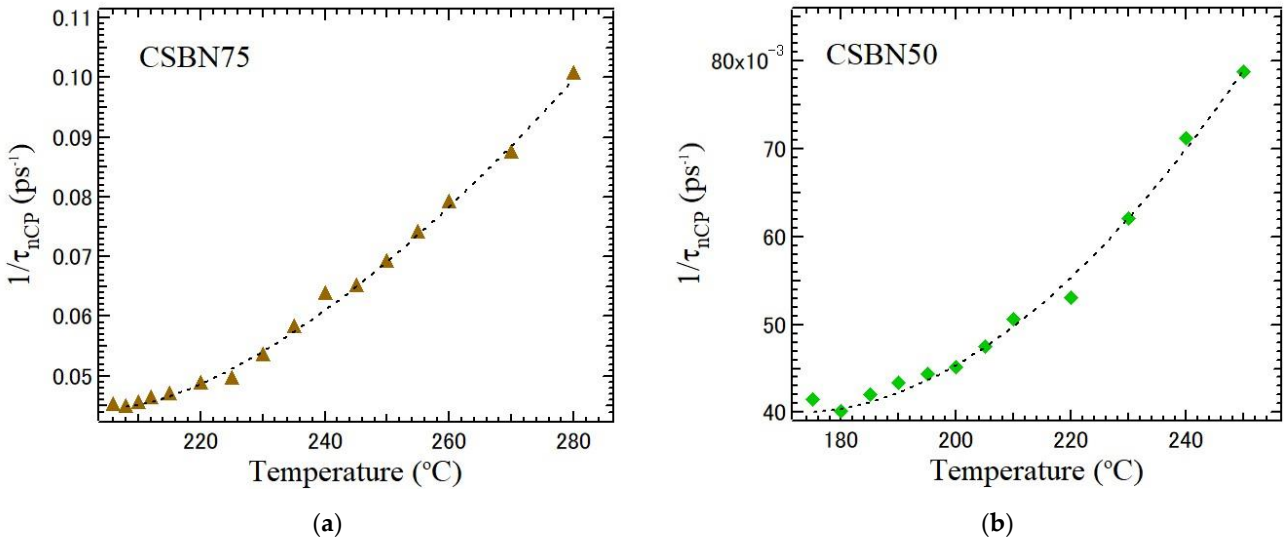

Figure 10. Difference in the temperature dependences of the stretched slowing down between (**a**) CSBN75 and (**b**) CSBN50 crystals. The brown triangles and green box are the observed values of CSBN75 and CSBN50, respectively. The dotted lines are fitted values to Equation (5) with β = 1.53 for CSBN75 and β = 1.88 for CSBN50.

The CBN28 content dependence of stretched index of five CSBN crystals is shown in Figure 11. The values of the diffuseness exponent determined by dielectric measurement using Equation (4) are also plotted for the comparison [27]. These exponents increase from 1.0 as the CBN28 content decreases. These similar dependences in the stretched index and diffuseness exponent indicate a crossover from a normal ferroelectric-like transition to a relaxor ferroelectric transition in CSBN.

Recently, the origin of the crossover from normal ferroelectric to relaxor in SBN and CSBN was discussed on the basis of site occupancy at A1 and A2 sites and residual entropy calculation [18]. The origin of the relaxor nature is attributed to the larger occupancy ratio of Sr:Ba at A2 sites. Differently from Sr ions, smaller Ca ions occupy only the A1 site. Therefore, the larger occupancy ratio decreases as the Ca content increases and the relaxor nature of SBN is suppressed. As another reason, lower excess oxygen in CSBN25 was also suggested [22]. To clarify the microscopic origin of the relaxor nature in TTB ferroelectrics, further studies are necessary.

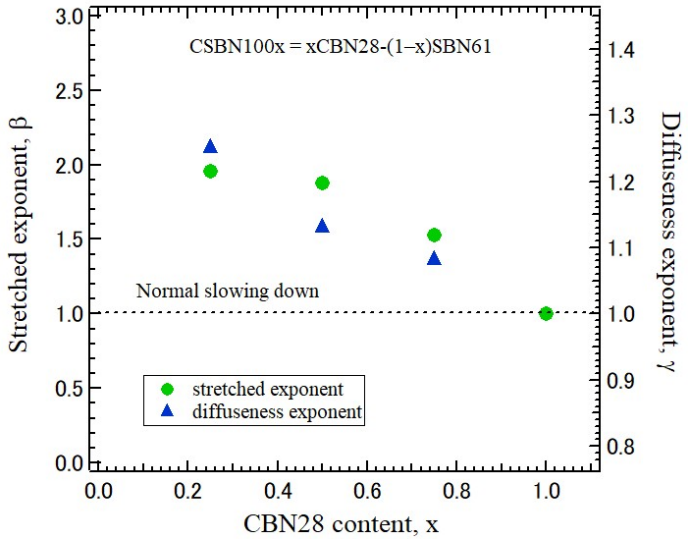

Figure 11. CBN28 content dependence of the exponent of stretched slowing down of Equation (5) in CSBN crystals. The values of the diffuseness exponent of dielectric constant of Equation (4) [27] are also plotted by way of the comparison.

4. Conclusions

Three dimensional relaxor ferroelectrics have been extensively studied with respect to their physical properties and to their origin of relaxor nature. Within this context, the results on uniaxial relaxor ferroelectrics have not completely been satisfactory. In this paper, the ferroelectric phase transitions of uniaxial ferroelectrics with tetragonal tungsten bronze structure were studied. Using Brillouin scattering spectroscopy, the elastic anomaly and a central peak (CP) with $A_1(z)$ symmetry were investigated. $Sr_xBa_{1-x}Nb_2O_6$ (SBN100x) with strong random fields (RFs) undergoes a relaxor ferroelectric phase transition, while $Ca_xBa_{1-x}Nb_2O_6$ (CBN100x) with weak RFs undergoes a nearly normal ferroelectric phase transition. The crossover from normal to relaxor ferroelectric behaviors was investigated in $x Ca_{0.28}Ba_{0.72}Nb_2O_6$-$(1-x)Sr_{0.61}Ba_{0.39}Nb_2O_6$ (CSBN100x) crystals. In a CBN28, crystal, the sharp elastic anomaly of the LA mode was observed in the vicinity of T_C. As the CBN28 content decreases, the anomaly of CSBN100x crystals becomes diffusive. A CSBN0 (SBN61) crystal shows a typical relaxor nature. In CBN28, the relaxation time determined from the width of a CP shows critical slowing down in the vicinity of T_C. While, as the CBN28 content decreases, slowing down of relaxation time in the vicinity of T_C becomes diffusive. In the gigahertz range, it was observed that two dynamical processes show a crossover from normal to relaxor nature in uniaxial ferroelectric CSBN100x crystals. The origins of the crossover from relaxor to normal ferroelectric phase transitions are discussed with regards to the difference in the A1 and A2 sites occupancies.

Author Contributions: Investigation, S.K., M.A., J.D. and W.K. All authors have read and agreed to the published version of the manuscript.

Funding: This research received no external funding.

Institutional Review Board Statement: Not applicable.

Informed Consent Statement: Not applicable.

Data Availability Statement: Data are contained within the articles.

Acknowledgments: The investigated crystals were grown at the Department of Oxide Single Crystals Technology in the Institute of Electronic Materials Technology, Warsaw under the leadership of T. Lukasiewicz. The authors are thankful to K. Matsumoto and K. Suzuki for the Brillouin scattering measurements.

Conflicts of Interest: The authors declare no conflict of interest.

References

1. Valasek, J. Piezo-Electric and Allied Phenomena in Rochelle Salt. *Phys. Rev.* **1921**, *17*, 475–481. [CrossRef]
2. Geusic, J.E.; Levinstein, H.J.; Rubin, J.J.; Singh, S.; Van Uitert, L.G. The Nonlinear Optical Properties of Ba2NaNb5O15. *Appl. Phys. Lett.* **1967**, *11*, 269–271. [CrossRef]
3. Bell, A.J.; Deubzer, O. Lead-free piezoelectrics—The environmental and regulatory issues. *MRS Bull.* **2018**, *43*, 581–587. [CrossRef]
4. Abrahams, S.C.; Jamieson, P.B.; Bernstein, J.L. Ferroelectric Tungsten Bronze-Type Crystal Structures. III. Potassium Lithium Niobate $K_{(6-x-y)}Li_{(4+x)}Nb_{(10+y)}O_{30}$. *J. Chem. Phys.* **1971**, *54*, 2355–2363. [CrossRef]
5. Ota, S.; Matsumoto, K.; Suzuki, K.; Kojima, S. Elastic anomaly and order-disorder nature of multiferroic barium sodium niobate studied by broadband Brillouin scattering. *IOP Conf. Ser. Mater. Sci. Eng.* **2014**, *54*, 012018. [CrossRef]
6. Lines, M.E.; Glass, A.M. *Principles and Applications of Ferroelectrics and Related Materials*; Clarendon Press: Oxford, UK, 1979.
7. Shvartsman, V.V.; Dec, J.; Miga, S.; Łukasiewicz, T.; Kleemann, W. Ferroelectric Domains in $Sr_xBa_{1-x}Nb_2O_6$ Single Crystals ($0.4 \leq \times \leq 0.75$). *Ferroelectrics* **2008**, *376*, 1–8. [CrossRef]
8. Aftabuzzaman, M.; Helal, M.A.; Paszkowski, R.; Dec, J.; Kleemann, W.; Kojima, S. Electric field and aging effects of uniaxial ferroelectrics $Sr_xBa_{1-x}Nb_2O_6$ probed by Brillouin scattering. *Sci. Rep.* **2017**, *7*, 11615. [CrossRef]
9. Eßer, M.; Burianek, M.; Klimm, D.; Mühlberg, M. Single crystal growth of the tetragonal tungsten bronze $Ca_xBa_{1-x}Nb_2O_6$ (x = 0.28; CBN-28). *J. Cryst. Growth* **2002**, *240*, 1–5. [CrossRef]
10. Song, H.; Zhang, H.; Jiang, Q.; Xu, X.; Lu, C.; Hua, X.; Wang, J.; Jiang, M. Growth, dielectric, ferroelectric and optical properties of $Ca_{0.28}Ba_{0.72}Nb_2O_6$ single crystals. *J. Cryst. Growth* **2006**, *290*, 431–435. [CrossRef]
11. Rubel, M.H.K.; Islam, M.S.; Mahmuda, U.S.M.; Rahaman, M.M.; Hossain, M.E.; Parvez, M.S.; Hossain, K.M.; Hossain, M.I.; Hossain, J.; Yamanaka, J.; et al. $Ca_xBa_{1-x}Nb_2O_6$ Ferroelectric Nanopowders for Ultrahigh-Density Optical Data Storage. *ACS Appl. Nano Mater.* **2018**, *1*, 6289–6300. [CrossRef]
12. Niemer, A.; Pankrath, R.; Betzler, K.; Burianek, M.; Müehlberg, M. Dielectric Properties and the Phase Transition of Pure and Cerium Doped Calcium-Barium-Niobate. *World J. Condens. Matter Phys.* **2012**, *2*, 80–84. [CrossRef]
13. Liu, H.; Xu, Y. The influence of sintering temperature on structural and electrical properties of x $(Ca_{0.28}Ba_{0.72})Nb_2O_6$-(1–x)$(Sr_{0.61}Ba_{0.39})Nb_2O_6$ ceramics. *J. Aust. Ceram. Soc.* **2020**, *56*, 1405–1411. [CrossRef]
14. Qi, Y.J.; Lu, C.J.; Zhu, J.; Chen, X.B.; Song, H.L.; Zhang, H.J.; Xu, X.G. Ferroelectric and dielectric properties of $Ca_{0.28}Ba_{0.72}Nb_2O_6$ single crystals of tungsten bronzes structure. *Appl. Phys. Lett.* **2005**, *87*, 082904. [CrossRef]
15. Suzuki, K.; Matsumoto, K.; Dec, J.; Łukasiewicz, T.; Kleemann, W.; Kojima, S. Critical slowing down and elastic anomaly of uniaxial ferroelectric $Ca_{0.28}Ba_{0.72}Nb_2O_6$ crystals with tungsten bronze structure. *Phys. Rev. B* **2014**, *90*, 064110. [CrossRef]
16. Lukasiewicz, T.; Swirkowicz, M.A.; Dec, J.; Hofman, W.; Szyrski, W. Strontium–barium niobate single crystals, growth and ferroelectric properties. *Crystal Growth* **2008**, *310*, 1464–1469. [CrossRef]
17. Kojima, S.; Aftabuzzaman, M.; Dec, J.; Kleemann, W. Brillouin Scattering Study of Ferroelectric Instability of Calcium Strontium Barium Niobate Crystals. *Proc. Ultrason. Electron. Symp.* **2022**, *3*, 89–90.
18. Liu, H.; Dkhil, B. Origin of the crossover from ferroelectric to relaxor in tetragonal tungsten bronzes. *J. Alloys Comp.* **2022**, *929*, 167314. [CrossRef]
19. Kojima, S. Gigahertz Acoustic Spectroscopy by Micro-Brillouin Scattering. *Jpn. J. Appl. Phys.* **2010**, *49*, 07HA01. [CrossRef]
20. Wieteska, K.; Wierzchowski, W.; Malinowska, A.; Lefeld-Sosnowska, M.; Świrkowicz, M.; Łukasiewicz, T.; Paulmann, C. Synchrotron diffraction topography of SrxBa1−xNb_2O_6 (SBN), $Ca_xBa_{1-x}Nb_2O_6$ (CBN) and mixed $(Ca_{0.28}Ba_{0.72})_y(Sr_{0.61}Ba_{0.39})_{1-y}Nb_2O_6$ (CSBN) crystals. *Radiat. Phys. Chem.* **2013**, *93*, 87–91. [CrossRef]
21. Wierzchowski, W.; Wieteska, K.; Malinowska, A.; Wierzbicka, E.; Romaniec, M.; Lefeld-Sosnowska, M.; Świrkowicz, M.; Łukasiewicz, T.; Sakowska, H.; Paulmann, C. "Ghost" segregation pattern and ferroelectric domains in mixed calcium-strontium-barium niobates. *X-ray Spectrom.* **2015**, *44*, 356–362. [CrossRef]
22. Malyshkina, O.; Ivanova, A.; Malyshkin, Y.; Folomeeva, A.; Shashkov, M.; Dec, J. Effect of Ca, Sr and Ba distribution on the relaxor properties of CSBN single crystals. *Ferroelectrics* **2017**, *511*, 76–81. [CrossRef]
23. Aftabuzzaman, M.; Dec, J.; Kleemann, W.; Kojima, S. Field dependent elastic anomaly in uniaxial tungsten bronze relaxors. *Jpn. J. Appl. Phys.* **2016**, *55*, 10TC01. [CrossRef]
24. Roth, M.; Mojaev, E.; Dul'kin, E.; Gemeiner, P.; Dkhil, B. Phase Transition at a Nanometer Scale Detected by Acoustic Emission within the Cubic Phase $Pb(Zn_{1/3}Nb_{2/3})O_3-xPbTiO_3$ Relaxor Ferroelectrics. *Phys. Rev. Lett.* **2007**, *98*, 265701. [CrossRef]
25. Hays, W.; Loudon, R. *Scattering of Light by Crystals*; Dover Publishing: New York, NY, USA, 1978.
26. Mühlberg, M.; Burianek, M.; Joschko, B.; Klimm, D.; Danilewsky, A.; Gelissen, M.; Bayarjargal, L.; Gorler, G.P.; Hildmann, B.O. Phase equilibria, crystal growth and characterization of the novel ferroelectric tungsten bronzes $Ca_xBa_{1-x}Nb_2O_6$ (CBN) and $Ca_xSryBa_{1-x-y}Nb_2O_6$ (CSBN). *J. Crys. Growth* **2008**, *310*, 2288–2294. [CrossRef]
27. Xu, Y.; Liu, H. Crystal structure effect on the phase transition of $(Ca_{0.28}Ba_{0.72})$x $(Sr_{0.61}Ba_{0.39})_{1-x}Nb_2O_6$ ceramics. *J. Mater. Sci. Mater. Electron.* **2020**, *31*, 5221–5226. [CrossRef]
28. Kim, M.S.; Wang, P.; Lee, J.H.; Kim, J.J.; Lee, Y.L.; Cho, S.H. Site Occupancy and Dielectric Characteristics of Strontium Barium Niobate Ceramics: Sr/Ba Ratio Dependence. *Jpn. J. Appl. Phys.* **2002**, *41*, 7042–7047. [CrossRef]
29. Kojima, S.; Aftabuzzaman, M.; Dec, J.; Kleemann, W. Ferroelectric phase transitions of uniaxial $Sr_{1-x}Ba_xNb_2O_6$ and their composition variation. *Jpn. J. Appl. Phys.* **2019**, *58*, SLLA02. [CrossRef]

30. Knauss, L.A.; Wang, X.M.; Toulouse, J. Polarization-strain coupling in the mixed ferroelectric $KTa_{1-x}Nb_xO_3$. *Phys. Rev. B* **1995**, *52*, 13261–13268. [CrossRef]
31. Rahaman, M.M.; Imai, T.; Kobayashi, J.; Kojima, S. Effect of Li-doping on polar-nanoregions in $K(Ta_{1-x}Nb_x)O_3$ single crystals. *Jpn. J. Appl. Phys.* **2015**, *54*, 10NB01. [CrossRef]
32. Uchino, K.; Nomura, S. Critical exponents of the dielectric constants in diffused-phase-transition crystals. *Ferroelectrics* **1982**, *44*, 55–61. [CrossRef]
33. Dong, X.L.; Kojima, S. Dielectric and resonance frequency investigations of phase transitions in Nb-doped PZT95/5 and 75/25 ceramics. *J. Phys. Conden. Matter.* **1997**, *9*, L171. [CrossRef]
34. Tsukada, S.; Kojima, S. Broadband light scattering of two relaxation processes in relaxor ferroelectric $0.93Pb(Zn_{1/3}Nb_{2/3})O_3-0.07PbTiO_3$ single crystals. *Phys. Rev. B* **2008**, *78*, 144106. [CrossRef]
35. Kojima, S.; Tsukada, S. Micro-Brillouin Scattering of Relaxor Ferroelectrics with Perovskite Structure. *Ferroelectrics* **2010**, *405*, 32. [CrossRef]
36. Kojima, S. Broadband Brillouin scattering study of ferroelectric instability of barium sodium niobate. *Condens. Matter Phys.* **2022**, *25*, 43702. [CrossRef]
37. Helal, M.A.; Aftabuzzaman, M.; Svirskas, S.; Banys, J.; Kojima, S. Temperature evolution of central peaks and effect of electric field in relaxor ferroelectric $0.83Pb(Mg_{1/3}Nb_{2/3})O_3$–$0.17PbTiO_3$ single crystals. *Jpn. J. Appl. Phys.* **2017**, *56*, 10PB03. [CrossRef]

Disclaimer/Publisher's Note: The statements, opinions and data contained in all publications are solely those of the individual author(s) and contributor(s) and not of MDPI and/or the editor(s). MDPI and/or the editor(s) disclaim responsibility for any injury to people or property resulting from any ideas, methods, instructions or products referred to in the content.